P10.20 CHARACTERISTICS OF SUPERCELLS SIMULATED WITH TORNADIC AND NON-TORNADIC RUC-2 PROXIMITY SOUNDINGS. PART III: COMPARISONS AT TORNADO-RESOLVING GRID SPACING

Jason Naylor* and Matthew S. Gilmore
University of North Dakota, Grand Forks, North Dakota

Richard L. Thompson and Roger Edwards
Storm Prediction Center, Norman, Oklahoma

1. INTRODUCTION

Although tornadoes have been studied extensively over the last forty years, many unanswered questions remain regarding their structure and development. Their highly destructive nature and relatively small temporal and spatial scales make them difficult to measure directly. In addition, it is difficult and expensive to deploy a network of instruments to analyze the air flow in and around a tornado. Because of these limitations, high resolution numerical models have been used extensively to study the structure and evolution of tornadic storms. Although these models have led to great advancements in the understanding of supercells, limitations in computing power have made it difficult to simulate a supercell at tornado-resolving resolution. To circumvent this difficulty, several studies have simulated tornado-like vortices (in the absence of the storm) by specifying the storm environment [e.g. Walko (1993), Trapp and Fiedler (1995), Lewellen et al. (1997), Markowski et al. (2003), Davies-Jones (2008), Lewellen and Lewellen (2007a,b)]. These studies have been able to make detailed observations of the tornadic vortices and demonstrate which processes may in fact produce tornadogenesis, however by prescribing aspects of the storm structure they are unable to simulate how these processes would evolve within a supercell.

There have been a handful of studies that have simulated the evolution of both the tornado and parent storm in an idealized three dimensional model. [e.g. Wicker and Wilhelmson (1995), Grasso and Cotton (1995), Gaudet and Cotton (2006a,b)]. These studies have all used somewhat idealized soundings with zero convective inhibition, a condition favorable for the traditional 'warm bubble' convective initiation technique to be successful. However, it has been shown that the majority of supercells occur in environments with at least small CIN [e.g. Rasmussen and Blanchard (1998)].

Advancements in computational power and numerical methodology now not only make it possible to simulate a supercell at tornado resolving resolution, but to also simulate numerous supercells at high resolution in a relatively short period of time. The purpose of this study is demonstrate that, when a strong enough convective initiation technique is used, an idealized model initiated with a tornadic proximity sounding will produce a tornadic supercell that evolves in a manner that agrees qualitatively with observations and theory. The preliminary results presented herein are part of a larger ongoing study aimed at investigating storm scale processes influential to tornadogenesis and tornadogenesis failure. The results from two simulations are presented, each initialized with a RUC-2 proximity sounding associated with a significantly tornadic supercell. In one simulation, a supercell forms that produces a tornado-like vorticity signature that extends from the surface to 3 km. In the second simulation, the resulting supercell fails to produce a strong, low-level vorticity signature. We argue that this non-tornadic case is an outlier and demonstrate that the storm that evolves in this case is atypical. The model setup and a description of the methodology are discussed in section 2. Results from both of the simulations are presented in section 3. Summary and future work is presented in section 4.

2. METHODOLOGY

2.1 Numerical Model

Idealized simulations were performed using version 14 of the Bryan Cloud Model (CM1). These simulations were performed on a Cray XT5 supercomputer (nicknamed Kraken) located at the National Institute for Computational Sciences. The model domain is 96 km x 96 km x 20 km with 100 m grid spacing in the horizontal and vertical. Simulations were carried out to 7200 s of cloud time. The model was run on 576 processors and took approximately 8 hrs of wall time to compete each simulation. The dynamics core utilizes the Klemp-Wilhelmson time-splitting technique with a large time step of 1 s and a small time step of 0.125 s. Lateral boundary conditions are wave-radiating and the upper and lower boundaries are free slip. A single moment, six class bulk microphysics parameterization from Gilmore et al. (2004) is used to represent precipitation

* *Corresponding author address*: Jason Naylor, Univ. of North Dakota, Dept. of Atmospheric Sciences, Grand Forks, ND, 58203;
email:jason.naylor@und.edu

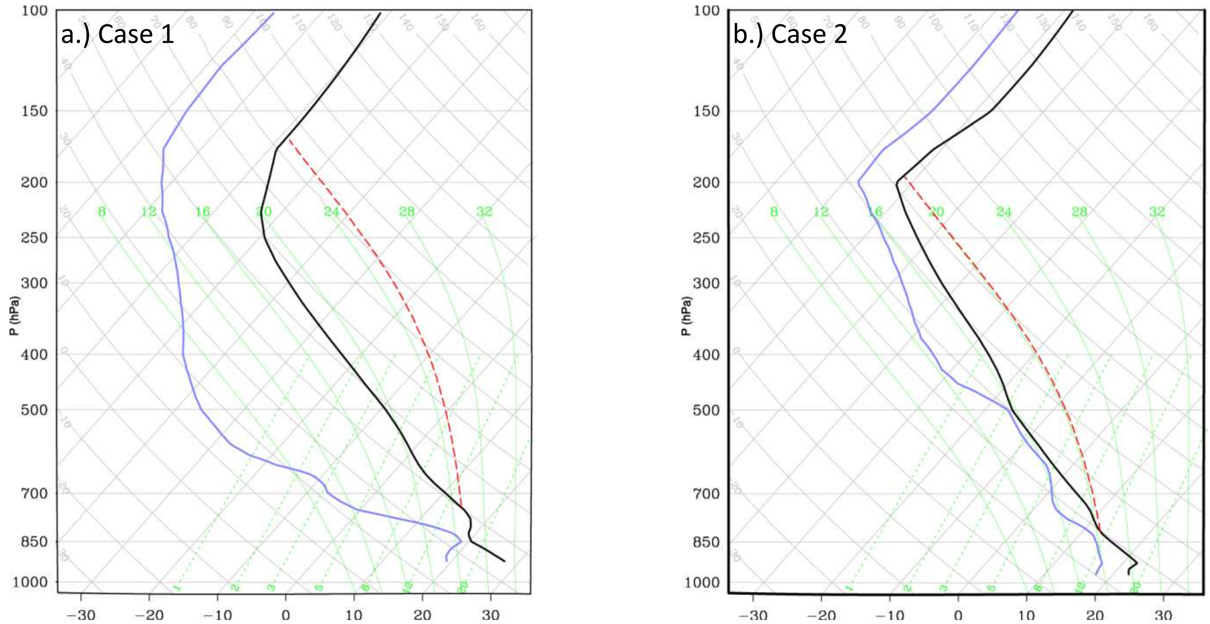

FIG. 1. Base state soundings for a.) Case 1 and b.) Case 2.

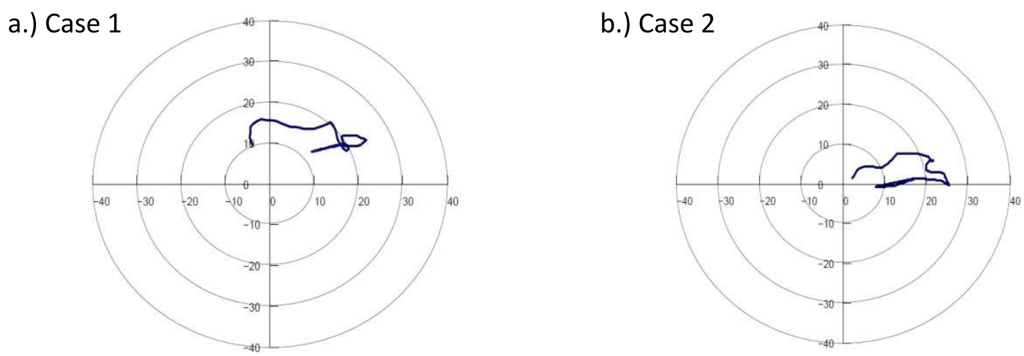

FIG. 2. Base state hodographs for a.) Case 1 and b.) Case 2. Units are m s^{-1}.

processes. Subgrid turbulence is computed using the Smagorinksy parameterization.

Due to the presence of capping inversions and strong shear in these soundings, the traditional warm bubble convective initiation method cannot be used. Instead, an updraft nudging technique was applied for the first 2700 s of cloud time. The nudging is performed over a 10 km x 10 km x 3 km sphere centered at z = 1.5 km. The updraft is accelerated at all points within the sphere where the updraft is less than 10 m s^{-1}. The nudging is strongest in the center of the sphere and decreases towards the edges. The magnitude of the nudging also decreases at all points as the updraft at that point approaches 10 m s^{-1}. This nudging technique helps the supercell to survive long enough to establish the vertical perturbation pressure gradient force that is essential for low-level updraft maintenance in the presence of a capping inversion (See Parts I and II for more discussion and analysis of the initiation technique).

Although this technique may be considered unrealistic, all initiation methods used in idealized models are somewhat unrealistic, including the commonly used warm bubble method (Loftus et al. 2008) It is believed that if the storms in the simulations are able to maintain their structure and intensity well after the updraft forcing is turned off, then the results (i.e. whether or not a storm produces a tornado) are not determined by the initialization technique, but rather by the storm environment. Storms are not analyzed until after the forcing is turned off.

2.2 Case Selection / Initial Conditions

The two cases presented in this study were chosen from a set of 134 simulations. Each of these simulations was initialized with one of the significantly tornadic soundings from Thompson et al. (2007). These 134 simulations were analyzed using information from standard output values recorded every 60 seconds of cloud time as well as horizontal and vertical cross section plots of storm structure created every 30 min from model history files. This analysis was performed to determine which simulations 1.) produced storms that maintained maximum updraft speeds (w_{max}) greater than 40 m s^{-1} until the end of the simulation, 2.) produced large vertical vorticity signatures at the surface indicative of a tornado and 3.) produced particularly long, strong lived tornadoes. The first criterion is being used to remove simulations with storms that were significantly weakened after the updraft forcing was turned off. A summary of the results is shown in Table 1.

Of the 134 simulations, 11 produced storms that maintained an updraft of greater than 40 m s^{-1} for the duration of the simulation. Of these 11 simulations, 10 produced storms with a maximum surface vertical vorticity of greater than 0.3 s^{-1}. The two cases presented in this study were chosen from this subset of 11. The first case (herein referred to as case 1) was chosen because it produced one of the stronger storms and also a large and long lived surface vorticity signature. The second case (herein case 2) was chosen because it is the only simulation that produced a strong, lived supercell that did not produce tornadic values of vertical vorticity at the surface.

Table 1. Summary of results from 100 m simulations initialized with the 134 significantly tornadic RUC-2 proximity soundings from Thompson et al. (2007).

Description	# of cases
w_{max} decreases rapidly after forcing turned off and storm dies	91
numerical instability (suspect waves are present in results)	18
w_{max} > 40 m s^{-1} for entire simulation	11
w_{max} < 40 m s^{-1} during the simulation (includes both weak storms and decaying storms	8
storm leaves domain before end of simulation	3
numerical instability (killed)	3
total	**134**

Case 1 is initialized with an environment characterized by CAPE of 4661 J kg^{-1}, 0-3 km storm relative environmental helicity (SREH) of 257 m^2 s^{-2} and 0-6 km vertical wind shear of 19.87 m s^{-1}. Case 2 has CAPE of 2073 J kg^{-1}, 0-3 km SREH of 145 m^2 s^{-2}, and 0-6 km vertical wind shear of 18.68 m s^{-1}. Soundings and hodographs for these two environments are shown in Figs 1 and 2. Both of these environments possess characteristics that previous studies have suggested to be favorable to tornadogenesis [e.g. Thompson et al. (2003), Rasmussen and Blanchard (1998)] including low LCL heights, and large values of CAPE. However, there are also many differences between the two environments, including the magnitudes of SREH, convective inhibition and also the vertical moisture profile. It is beyond the scope of the current study to analyze the full parameter space of the two storm environments and identify environmental characteristics responsible for differences in overall storm structure.

2.3 Defining a Vortex as a Tornado

By assuming a tornado can be represented as a Rankine vortex, cyclostrophic balance arguments can be used to define the criteria used for a simulated vortex to be classified as a tornado. A tornado is said to be present in the simulation if the following features are found within the surface mesocyclone: 1.) a pressure deficit of 5 hPa, 2.) vertical vorticity greater than 0.3 s^{-1}, and 3.) winds exceeding 30 m s^{-1}. In the following discussion of results, the term ‘surface’ refers to values at the lowest scalar level (z = 50 m).

3. RESULTS

3.1 Overview

a. Case 1

By t=3600 s, the storm in Case 1 has developed features indicative of a supercell (Fig. 3a). The storm exhibits a hook shaped appendage in the simulated radar reflectivity factor field as well as a strong, quasi-steady updraft immediately to the south of the main precipitation core, and a region of vertical vorticity coincident with the updraft. Maximum updraft values in the domain are over 80 m s^{-1}. By t=4100 s, the hook echo appears to be impinging on the main updraft, causing it to narrow somewhat along the minor axis (Fig. 3b). At lower levels, the RFD has become well developed (not shown). By t=4250 s, the RFD has increased in size and downdrafts have developed immediately to the west of the updraft, creating the divided mesocyclone documented by previous studies (Fig. 3c). Over the next 100 s, the area of this downdraft increases (Fig. 3d). By this time, ζ_{max} has moved from the center of the updraft to the edge of the updraft / downdraft boundary (not shown), indicative of a transition to the tornadic phase.

Time-height cross sections of vertical velocity and vertical vorticity are shown in Fig. 4. These plots

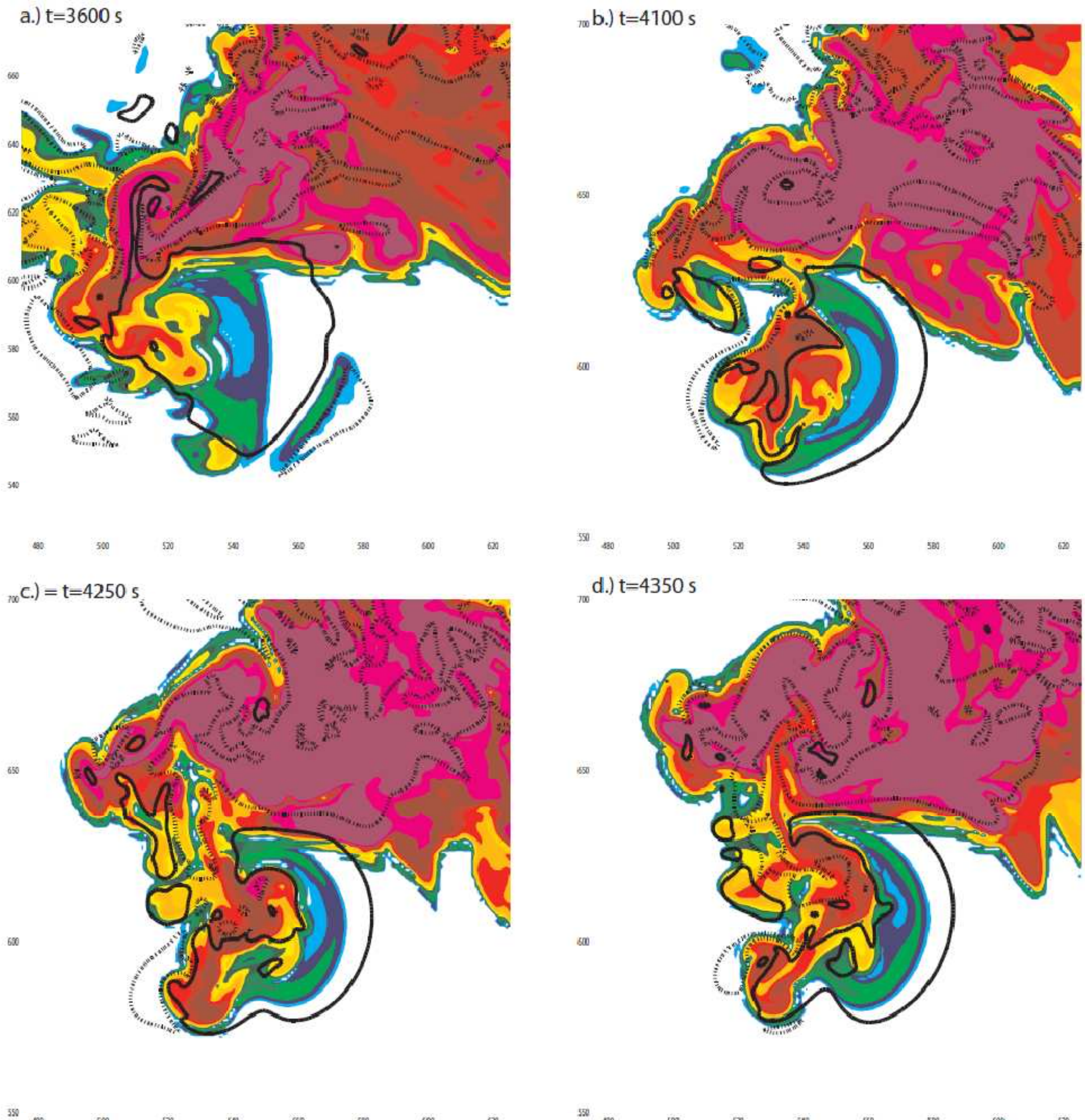

FIG. 3. Horizontal cross sections at z = 2950 m for Case 1. Filled contours are simulated radar reflectivity factor (dBZ), solid black contours are w > 10 m s^{-1} and dashed black contours are w < -5 m s^{-1}.

reveal large values of vertical vorticity present at all levels from t=3600 s to t=5000 s, with larger values first appearing aloft. These values are an order of magnitude larger than the typically used threshold for mesocyclones. Wicker and WIlhelmson (1995) also showed large values of vertical vorticity throughout the lowest 6 km; however the magnitudes of the values shown here are more than double those shown in their study. Upon closer inspection of the large ζ values aloft, it seems these values occur on the north-northwest edge of the main updraft and also in the hook echo. In both cases, they are concentrated in areas with a radius of only a few hundred meters.

Fig. 4a shows the presence of two distinct updraft 'pulses'. The first occurs at approximately t = 3900 s and extends from 3 km to 9 km. This pulse immediately precedes the development of large vertical vorticity centered at z=5.5 km. The second pulse begins around t=4400 s near 1.5 km and extends upwards to roughly 8 km by t=4600 s. This pulse seems to occur in conjunction with the development of large vertical vorticity near the surface between t=4350 s and t=4500 s, which agrees with the results of Wicker and Wilhelmson (1995).

b. Case 2

Midlevel storm structure at t=3000 s is shown in Fig 5a. At this time, the storm has a prominent hook shaped appendage in the simulated radar reflectivity. The updraft exhibits a two-celled structure. Both sections of the updraft are collocated with regions of $\zeta > 0.02\ s^{-1}$. Detailed evolution of the storm over the next 600 s cannot be provided, since history files were only recorded every 600 s until t=3600, after which time the frequency of model output was

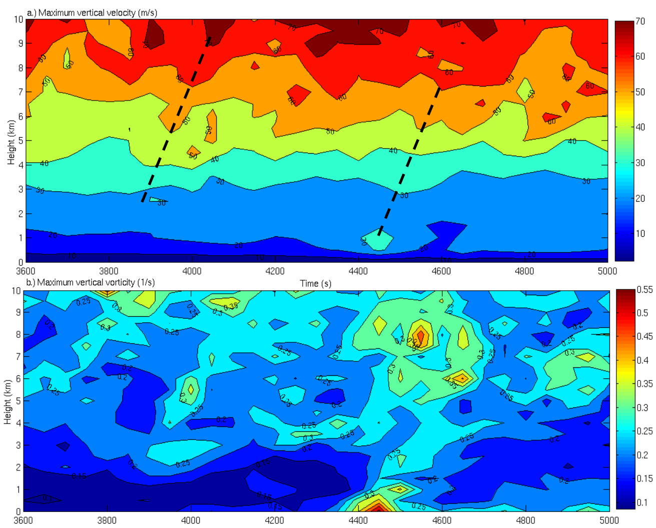

FIG. 4. Time height cross-sections of (a) maximum vertical velocity and (b) maximum vertical vorticity for case 1.

increased. By t=3600 s, the structure of the storm has changed significantly (Fig. 5b). The main updraft on the southern flank has weakened and the hook echo has narrowed. Over the next 1800 s, the storm undergoes an occlusion and evolves in a way that is qualitatively similar to the conceptual model developed in Adlerman et al. (1999). After the occlusion, the surface gust front propagates eastward ahead of the storm, separating the low level updraft from the midlevel updraft. The midlevel updraft develops a two-cell structure that is oriented mainly in the east-west direction (Fig 5c). Over time, the eastern half of the updraft intensifies, while the western portion decays.

By t=5400 s, the two-cell updraft has evolved into a singular updraft located on the southern flank of the storm (Fig. 5d). The updraft in this storm is smaller and weaker than the updraft in case 1, with a domain maximum value of about 60 m s^{-1}. The surface gust front remains well ahead of the storm. Over the next 800 s as the storm continues to reorganize, a new gust front develops well behind the original gust front (not shown). Updrafts along this new gust front appear weaker than the updrafts along the original gust front. It seems as if the storm has cut itself off from surface inflow after the occlusion and is now being fueled primarily by air from aloft.

Time-height cross sections of updraft and vertical vorticity show that the magnitudes of these values are smaller than those in case 1 at all levels from 0-10 km (Fig 6). An updraft pulse is present at t=3600 s between 4 km and 9 km. As in case 1, this pulse precedes the development of increased vertical vorticity aloft, particularly near 9 km. Fig. 6a shows that the updraft experienced a significant weakening between t=4500 and t=5400 s. At this time, the storm was reorganizing after the occlusion. By t=5400 s, the updraft has regained its intensity.

As in case 1, values of vertical vorticity are larger aloft than near the surface. There are four instances when ζ exceeds 0.1 s^{-1} at the surface. The first two instances occur around t=4000 s and t=4300 s, shortly after the storm begins to occlude. The latter two occur after the occlusion, at which time the gust front has surged well eastward of the storm.

3.2. Evolution of Surface Rotation

a. Case 1

By t=3600 s, Case 1 has developed a region of vertical vorticity and updraft co-located along the gust front with a maximum ζ of 0.11 s^{-1} (Fig. 7a). There is a slight kink in the position of the gust front as well as the updraft field, indicating the development of a circulation center (labeled A in Fig. 7a). Just to the north, there is a second kink in the position of the gust front where vertical vorticity is increasing (labeled B in Fig. 7a). This second circulation center is developing in a region where inflow from the north is parallel to the gust front. As time progresses, the circulation at A strengthens and develops a horse-shoe shaped updraft, while the circulation at B also continues to strengthen and develops a similar form.

By t=3900 s, the original surface mesocyclone (A) has moved southwest along the gust front and weakened while the circulation at point B has also moved south, but has strengthened and becomes the dominant circulation center (Fig. 7b). This mesocyclone has ζ_{max} of 0.13 s^{-1}. There is also a new circulation center (labeled C in Fig. 7b) that has developed to the north. This seemingly cyclic process of generating small, intense regions of circulation continues to repeat with a frequency of just a few hundred seconds. Similar phenomenon have been observed by Brooks et al. (1994) and Wicker and Wilhelmson (1995). However, the vorticity values in Brooks et al. are an order of magnitude smaller, most likely owing to the coarser resolution used in their simulations.

Between t=4050 s and t=4100 s, the mesocyclone at point C undergoes rapid intensification (not shown). The updraft gains a horseshoe shaped appearance and ζ_{max} increases to 0.14 s^{-1}. In addition, the

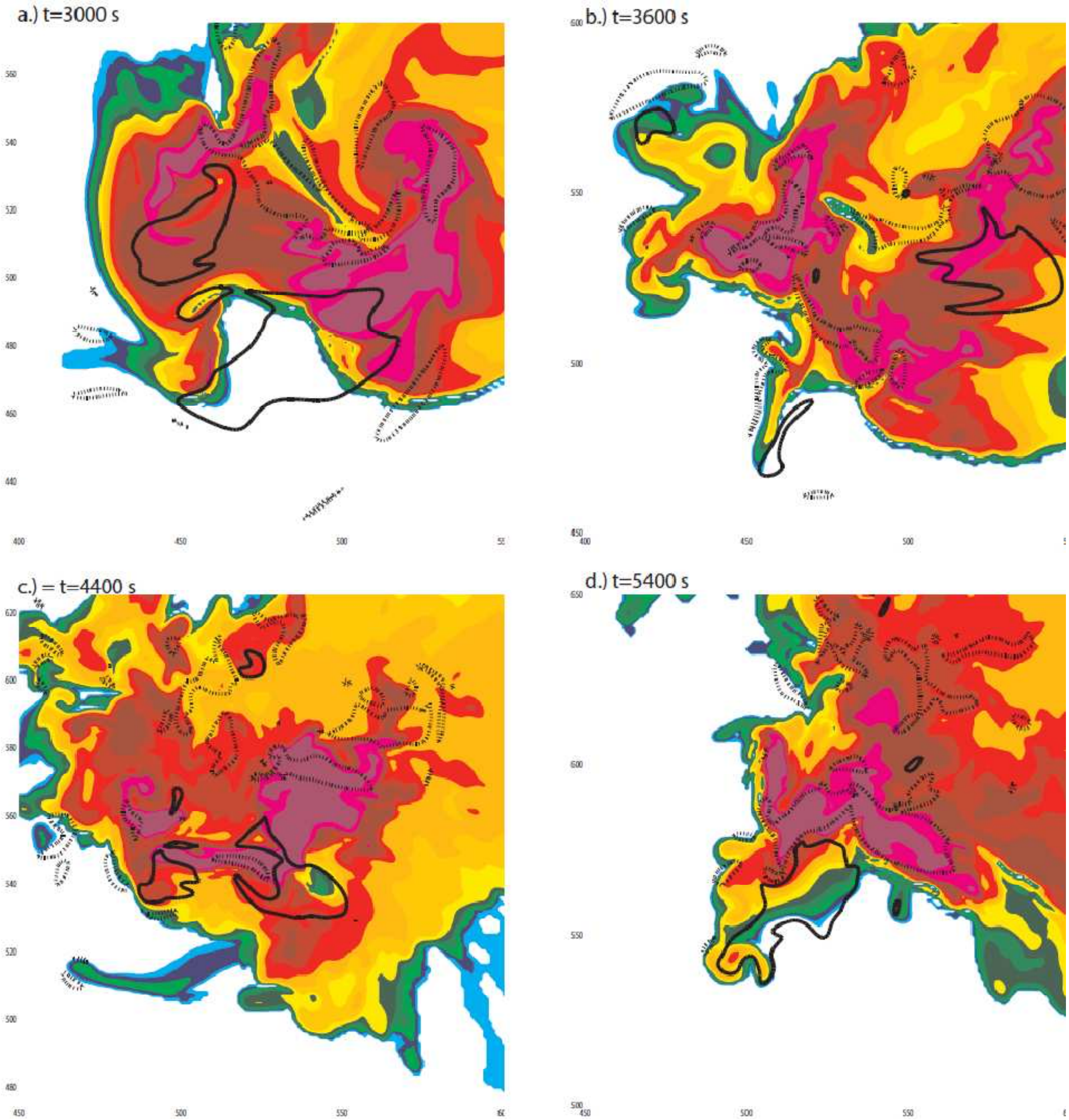

FIG. 5. Horizontal cross sections at z = 2950 m for Case 2. Filled contours are simulated radar reflectivity factor (dBZ), solid black contours are w > 10 m s^{-1} and dashed black contours are w < -5 m s^{-1}.

mesocyclone has developed a divided structure, with a downdraft located within the horseshoe shaped updraft. This downdraft has a minimum vertical velocity of about -1.36 m s^{-1}. However, like the previous circulation centers, it too begins to weaken and move to the south.

By t=4300 s, a new circulation center has evolved to the north (herein referred to as D) (Fig. 7c). Features of this structure are similar to the three previous events; a horseshoe shaped updraft collocated with a region of vertical vorticity greater than 0.1 s^{-1} (ζ_{max} is ~ 0.15 s^{-1}), and a divided structure, with a downdraft just to the east of the maximum updraft. A major difference between the circulation at D and the previous circulation centers is the large region of vertical vorticity just to the west that is being advected towards the center of circulation.

Over the next 100 s, vorticity rapidly increases, along with the wind speed and the circulation reaches tornadic strength by t=4400 s (Fig. 7d). By t=4440 s the tornado has reached peak intensity. The vortex has a surface pressure drop of 22 mb, maximum storm relative winds of 47 m s^{-1} and a peak vorticity of

0.61 s^{-1}. At this time the gust front is over 1 km to the east of the tornado. The surface wind field seems to suggest that the tornado has been entirely cut off from inflow air. By t=4600 s, the circulation has weaken to the point where it no longer meets the criteria to be defined as a tornado.

b. Case 2

At t=3600 s, vertical vorticity is being generated along the gust front, and a kink in the gust front is present near the tip of the 30 dBZ contour (labeled 'A' in Fig. 8a). Over the next 400 s, the updraft at A becomes more contorted until it assumes a horseshoe shaped structure similar to the features discussed in case 1 (Fig. 8b). There is also a new center forming to the north in the region of stronger updraft (point B). By t=4100 s, the original circulation center at point A begins to weaken, while the circulation at B increases. This process is similar to that discussed in case 1, with new circulation centers strengthening and decaying every few hundred seconds.

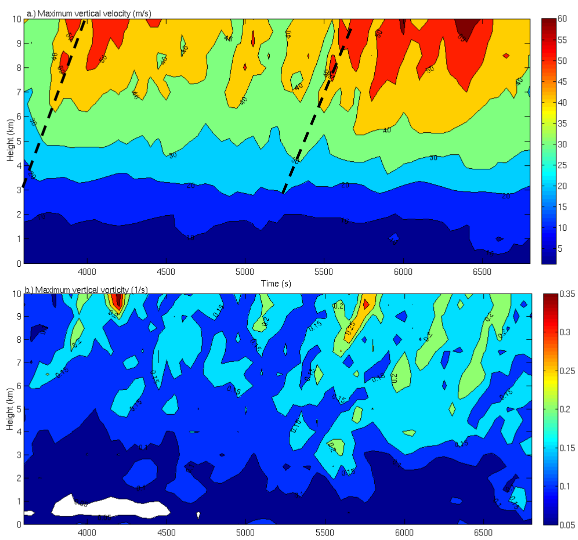

FIG 6. Same as Fig. 4, except for case 2.

By t=4300 s, the circulation has strengthened and a downdraft is now present within the mesocyclone at point B (Fig. 8c). At this time, maximum ζ in the mesocyclone is 0.11 s^{-1}. Two new circulations are forming to the north (labeled 'C' and 'D' in Fig. 8c). The circulation at point D is located within the 30 dBz contour. By t=4400 s, the circulation at point B decays and ζ_{max} becomes associated with the circulation at point D. This new circulation has ζ_{max} of 0.06 s^{-1}.

Over the next 800 s, the gust front begins to pull ahead of the 30 dBZ contour as the storm reorganizes after the occlusion. By t=5200 s, the gust front is nearly 2 km to the east of the 30 dBZ contour. (Fig. 8d). Regions of vorticity continue to develop along the gust front after this time, however these circulations are well ahead of the midlevel updraft.

3.3 RFD Thermodynamics

The thermodynamic properties of downdrafts occurring in close proximity to the surface mesocyclone were investigated to determine if strong differences in the surface psuedoequivalent potential temperature (θ_{ep}) fields between the two cases existed. This analysis was done by first locating the maximum value of ζ at the surface. Checks were performed to make sure this value was associated with the mesocyclone. Next, a 6 km x 6 km box was placed around the location of ζ_{max}. The minimum, maximum, and average values of θ_{ep} were calculated at points inside this box. The values were filtered to only consider points with w < -0.5 m s^{-1}. This was done to filter out grid points on the inflow side of the gust front. The base state θ_{ep} was then subtracted from these values to determine the magnitude of the θ_{ep} deficit (i.e. at the surface).

In case 1, the magnitude of the deficit is relatively large prior to tornadogenesis (Fig. 9a), with the largest value of θ_{ep} being nearly 10 k smaller than the base state at t=4000 s. However, just prior to tornadogenesis (between t=4200 and t=4300), the maximum θ_{ep} deficit increases to roughly -5 K. The average deficit remains relatively unchanged, suggesting that the majority of downdraft parcels continue to transport air to the surface with relatively small θ_{ep}. By the time the tornado forms at t=4350 s, the average, maximum, and minimum θ_{ep} deficits are at a local maximum. Over the next 100 s, as the tornado approaches peak intensity at t=4450, these values all decrease. More analysis is needed to determine how the θ_{ep} fluctuations effect the life cycle of the tornado.

In case 2, the deficits are small throughout the simulation (Fig. 9b). In fact, there are some instances when downdrafts are transporting air with larger θ_{ep} to the surface. It is interesting that case 2 has a relatively 'warm' cold pool, yet the gust front propagates well ahead of the storm. This seems likely to be related to the weak winds at the surface.

4. SUMMARY

A suite of 134 high resolution simulations were performed using RUC-2 proximity soundings associated with significant tornadoes (Thompson et al. 2007). Of the 134 simulations, 11 produced strong, long lived supercells that maintained their intensity until the end of the simulation. Of these 11, 10 produced large surface vertical vorticity values indicative of tornadoes, while one did not. Results from one of the tornadic simulations (case 1) were presented, as well as results from the non-tornadic simulation (case 2).

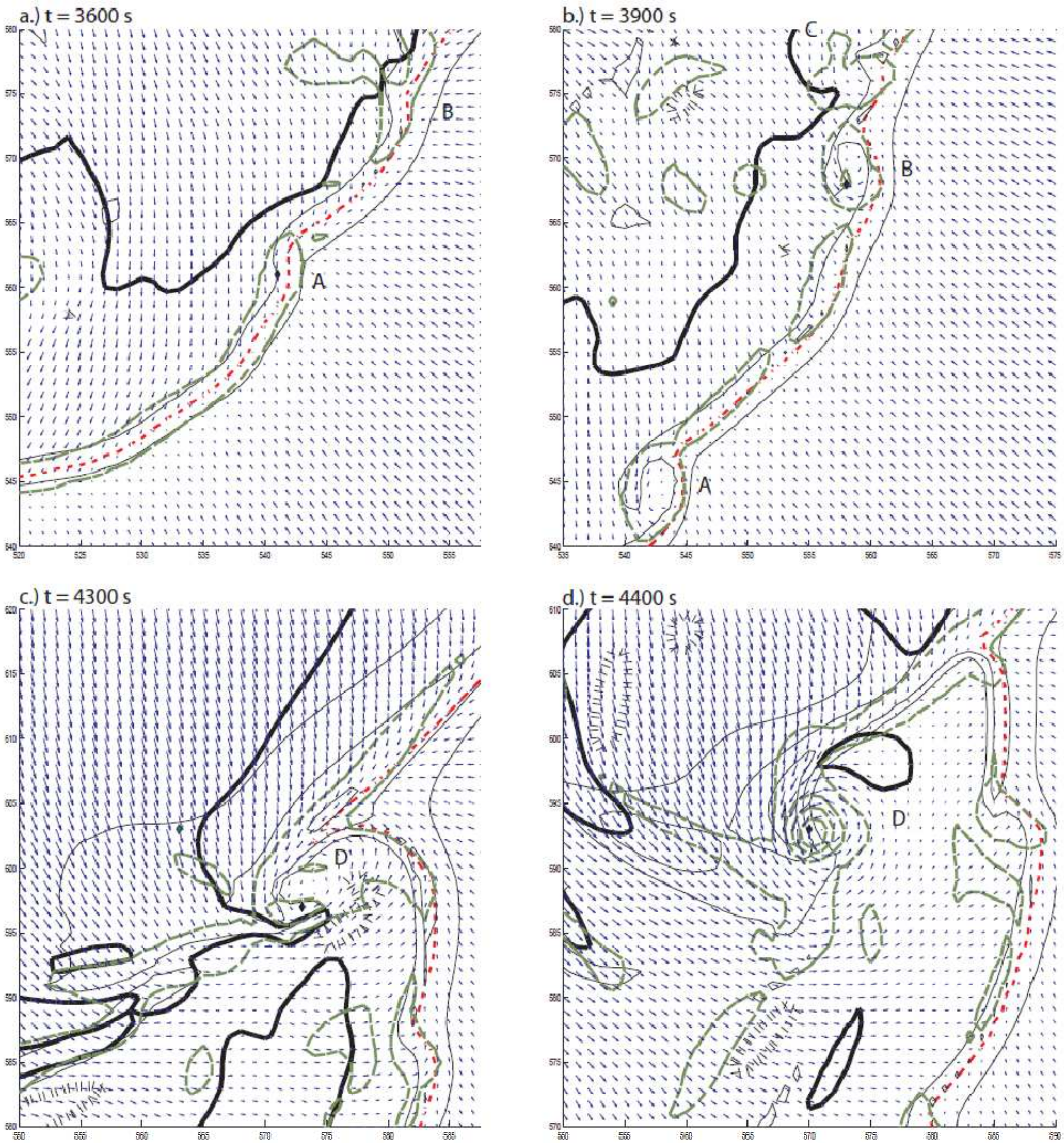

FIG 7. Overview of storm structure for case 1 at z=50 m. Thick black line is the 30 dBZ contour, thin black line is w > 1 m s^{-1} contour, red dashed line is -1 K potential temperature perturbation, hatched black line is w < -1 m s^{-1} and the green line is contours of vertical vorticity starting at 0.01 s^{-1} with an interval of 0.1 s^{-1}.

Both tornadic and non-tornadic supercells produced small, localized areas of enhanced circulation at the surface. These circulation centers migrated southeastward along the rear flank gust front while new circulation centers developed to the north where inflow was parallel to the gust front. In both cases, this process repeated itself with a frequency of a few hundred seconds.

It seems that one of the main differences between the two simulations was the presence of near surface downdrafts. In case 1, tornadogenesis seems to occur in conjunction with strong downdrafts present around the mesocyclone. Some of these downdrafts were collocated with $\zeta > 0.01$ s^{-1}, suggesting this vertical vorticity may have been transported to

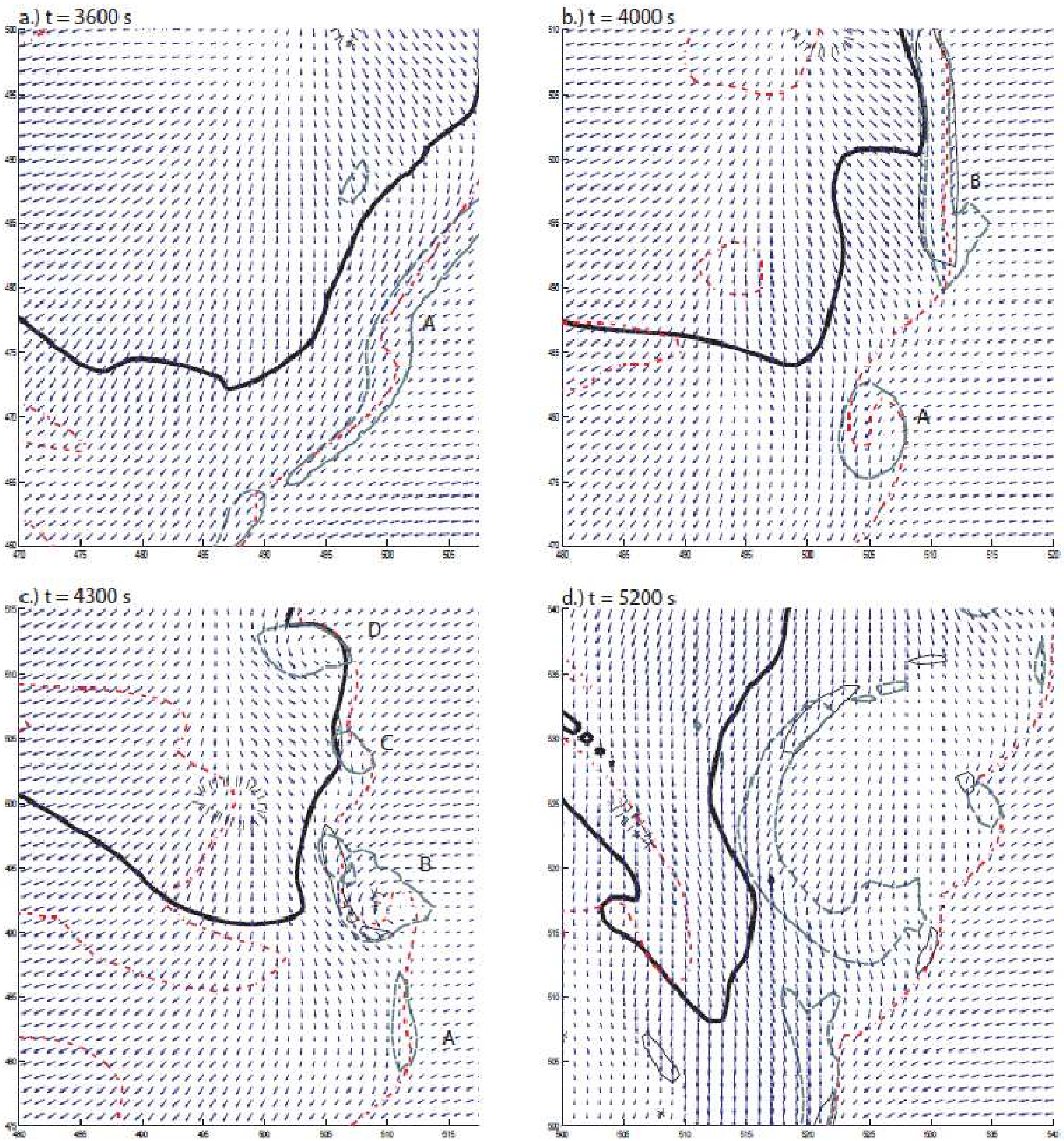

FIG. 8. Same as Fig. 7, except for case 2

the surface by downdrafts. However, trajectory analysis and Lagrangian vorticity calculations are needed to verify this conjecture. Just prior to tornadogenesis, it appears as if this vertical vorticity was being advected into the mesocyclone by the storm outflow. In case 2, downdrafts were weaker and more sporadic, and were not co-located with significant values of vertical vorticity.

From the analysis presented, it is not possible to determine why case 2 did not produce a tornado. However, it may be possible that the occlusion and subsequent weakening of the midlevel updraft was detrimental to the formation of intense near ground circulation in the simulation. Burgess et al. (1982) suggested that only 24% of mesocyclones experience cyclic occlusion. Thus, in that sense, case 2 can in fact be considered atypical.

It is also possible that case 2 failed to produce a tornado in the idealized model because an essential process was not represented in the idealized framework. For example, several studies have shown that tornadogenesis can be aided by the development of vorticity along a thermal boundary [e.g. Maddox et al. (1980), Markowskiet al. (1998)]. Also absent from the model is the transport of angular momentum by rain curtains, which has been shown by Davies-Jones (2008) to be able to instigate tornadogenesis. This process may have been important to case 2 because of the strong capping inversion present in the sounding. This cap may have prevented downdrafts from penetrating to the surface and transporting vertical vorticity from aloft.

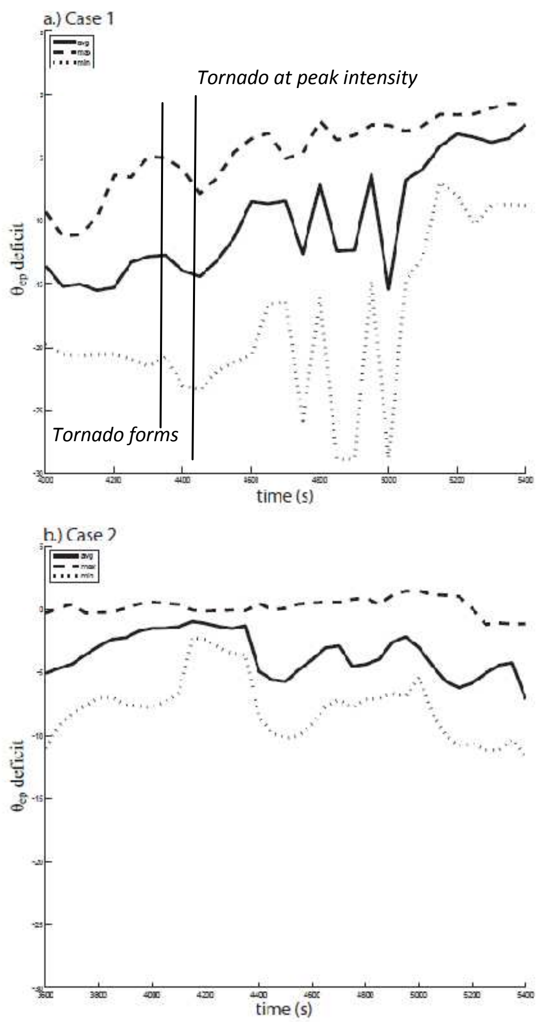

FIG. 9. Maximum, minimum, and average psuedoequivalent potential temperature (θ_{ep}) deficits of downdrafts at the surface for a.) case 1 and b.) case 2.

5. FUTURE WORK

Analysis of these two cases is ongoing. Trajectory anaylsis, circulation calculations, and vorticity budgets are currently underway. Analysis of the other nine successful cases is also planned in the near future.

In addition to analyzing the 134 simulations already performed, work is planned to test if varying the strength and duration of the convective initiation technique will produce more successful cases.

Currently, only RUC-2 proximity soundings from significantly tornadic events have been simulated. We plan on performing an equal number of simulations form the non-tornadic group of proximity soundings. Our current results suggest that the significantly tornadic soundings generally produce tornadoes in the model. We hypothesize that the majority of high resolution simulations using non-tornadic soundings will fail to produce tornadoes.

ACKNOWLEDGEMENTS

This work was supported by NSF grant. AGS-0843269. Partial travel support was provided through NSF grant EPS-0814442. Computer resources were provided through Teragrid allocation TG-MCA94P023.

REFERENCES

Adlerman, E. J., K. K. Droegemeier, R. Davies-Jones, 1999: A numerical simulation of cyclic mesocyclogenesis. *J. Atmos. Sci.*, **56**, 2045-2069.

Burgess, D. W., V. T. Wood, and R. A. Brown, 1982: Mesocyclone evolution statistics. Preprints, *12th Conf. on Severe Local Storms*, San Antonio, TX, Amer. Meteor. Soc., 422-424.

Brooks, H. E., C. A. Doswell III, and R. B. Wilhelmson, 1994: The role of midtropospheric winds in the evolution and maintenance of low-level mesocyclones. *Mon. Wea. Rev.*, **122**, 126-136.

Davies-Jones, R., 2008: Can a descending rain curtain in a supercell instigate tornadogenesis barotropically? *J. Atmos. Sci.*, **65**, 2469-2497.

Gaudet, B. J., and W. R. Cotton, 2006a: Low-level mesocyclonic concentration by nonaxisymmetric transport. Part I: Supercell and Mesocyclone evolution. *J. Atmos. Sci.*, **63**, 1113-1133.

____, and ____, 2006b: Low-level mesocyclonic concentration by nonaxisymmetric transport. Part II: Vorticity dynamics. *J. Atmos. Sci.*, **63**, 1134-1150.

Gilmore, M. S., J. M. Straka, and E. N. Rasmussen, 2004: Precipitation and evolution sensitivity in simulated deep convective storms: Comparisons between liquid-only and simple ice and liquid phase microphysics. *Mon. Wea. Rev.*, **132,** 1897-1916.

Grasso, L. D., and W. R. Cotton, 1995: Numerical simulation of a tornado vortex. *J. Atmos. Sci.*, **52**, 1192-1203.

Lewellen, D.C, and W. S. Lewellen, 2007a: Near-surface intensification of tornado vortices. *J. Atmos. Sci.*, **64**, 2176-2194.

____, and ____, 2007b: Near-surface vortex intensification through corner flow collapse. *J. Atmos. Sci.*, **64**, 2195-2209.

Loftus, A. M., D. B. Weber, and C. A. Doswell III, 2008: Parameterized mesoscale forcing mechanisms for initiating numerically simulated isolated multicellular convection. *Mon. Wea. Rev.*, **136**, 2408-2421.

Maddox, R. A., L. R. Hoxit, and C. F. Chappell, 1980: A study of tornadic thunderstorms interacting with thermal boundaries. *Mon. Wea. Rev.*, **108**, 322-336.

Markowski, P. M., E. N. Rasmussen, and J. M. Straka, 1998: The occurrence of tornadoes in supercells interacting with boundaries during VORTEX-95. *Wea. Forecasting*, **13**, 852-859.

____, J. M. Straka, and E. N. Rasmussen, 2003: Tornadogenesis resulting from the transport of circulation by a downdraft: Idealized numerical simulations. *J. Atmos. Sci.*, **60**, 795-823.

Rasmussen, E. N., and D. O. Blanchard, 1998: A baseline climatology of sounding-derived supercell and tornado forecast parameters. *Wea. Forecasting*, **13,** 1148-1164.

Thompson, R. L., R. Edwards, J. A. Hart, K. L. Elmore, and P. M. Markowski, 2003: Close proximity soundings within supercell environments obtained from the rapid update cycle. *Wea. Forecasting*, **18**, 1243-1261.

____, C. M. Mead, and R. Edwards, 2007: Effective storm-relative helicity and bulk shear in supercell thunderstorm environments. *Wea. Forecasting*, **22**, 102-115.

Trapp, R. J., and B. H. Fiedler, 1995: Tornado-like vortexgenesis in a simplified numerical model. *J. Atmos. Sci.*, **52**, 3757-3778.

Walko, R. L., 1993: Tornado spin-up beneath a convective cell: Required basic structure of the near-field boundary layer winds. *The Tornado: Its Structure, Dynamics, Prediction, and Hazards, Geophys. Monogr.*, No 79, Amer. Geophys. Union, 89-95.

Wicker, L. J. and R. B. Wilhelmson, 1995: Simulation and analysis of tornado development and decay within a three-dimensional supercell thunderstorm. *J. Atmos. Sci.*, **52**, 2675-2703.